IJMMM International Journal of Minerals, Metallurgy and Materials 矿物冶金与材料学报（英文版）

Effect of samarium on the N_2 selectivity of $Sm_xMn_{0.3-x}Ti$ catalysts during selective catalytic reduction of NO_x with NH_3

Shengyang Zhang, Bolin Zhang, Boyu Wu, Bo Liu, and Shengen Zhang

Cite this article as:
Shengyang Zhang, Bolin Zhang, Boyu Wu, Bo Liu, and Shengen Zhang, Effect of samarium on the N_2 selectivity of $Sm_xMn_{0.3-x}Ti$ catalysts during selective catalytic reduction of NO_x with NH_3, *Int. J. Miner. Metall. Mater.*, 30(2023), No. 4, pp. 642-652. https://doi.org/10.1007/s12613-021-2348-5

View the article online at SpringerLink or IJMMM Webpage.

Articles you may be interested in

IJMMM WeChat

QQ author group

International Journal of Minerals, Metallurgy and Materials
Volume 30, Number 4, April 2023, Page 642
https://doi.org/10.1007/s12613-021-2348-5

Effect of samarium on the N_2 selectivity of $Sm_xMn_{0.3-x}Ti$ catalysts during selective catalytic reduction of NO_x with NH_3

Shengyang Zhang[1)], *Bolin Zhang*[1,2),✉], *Boyu Wu*[1)], *Bo Liu*[1)], *and Shengen Zhang*[1),✉]

1) Institute for Advanced Materials and Technology, University of Science and Technology Beijing, Beijing 100083, China
2) Shunde Innovation School, University of Science and Technology Beijing, Foshan 528399, China
(Received: 13 April 2021; revised: 5 September 2021; accepted: 6 September 2021)

Abstract: This work aims to study the improvement effect of Sm on Mn-based catalysts for selective catalytic reduction (SCR) of NO with NH_3. A series of $Sm_xMn_{0.3-x}Ti$ catalysts (x = 0, 0.1, 0.15, 0.2, and 0.3) were prepared by co-precipitation. Activity tests indicated that the $Sm_{0.15}Mn_{0.15}Ti$ catalyst showed superior performances, with a NO conversion of 100% and N_2 selectivity above 87% at 180–300°C. The characterizations showed that Sm doping suppressed the crystallization of TiO_2 and Mn_2O_3 phases and increased the specific surface area and acidity. In particular, the surface area increased from 152.2 $m^2 \cdot g^{-1}$ for $Mn_{0.3}Ti$ to 241.7 $m^2 \cdot g^{-1}$ for $Sm_{0.15}Mn_{0.15}Ti$. These effects contributed to the high catalytic activity. The X-ray photoelectron spectroscopy (XPS) results indicated that the relative atomic ratios of Sm^{3+}/Sm and O_β/O of $Sm_{0.15}Mn_{0.15}Ti$ were 76.77at% and 44.11at%, respectively. The presence of Sm contributed to an increase in surface-absorbed oxygen (O_β) and a decrease in Mn^{4+} surface concentration, which improved the catalytic activity. In the results of hydrogen temperature-programmed reduction (H_2-TPR), the presence of Sm induced a higher reduction temperature and lower H_2 consumption (0.3 $mmol \cdot g^{-1}$) for the $Sm_{0.15}Mn_{0.15}Ti$ catalyst compared to the $Mn_{0.3}Ti$ catalyst. The decrease in Mn^{4+} weakened the redox property of the catalysts and increased the N_2 selectivity by suppressing N_2O formation from NH_3 oxidation and the nonselective catalytic reduction reaction. The *in situ* diffuse reflectance infrared Fourier transform spectra (DRIFTs) revealed that NH_3-SCR of NO over the $Sm_{0.15}Mn_{0.15}Ti$ catalyst mainly followed the Eley–Rideal mechanism. Sm doping increased surface-absorbed oxygen and weakened the redox property to improve the NO conversion and N_2 selectivity of the $Sm_{0.15}Mn_{0.15}Ti$ catalyst.

Keywords: manganese oxides; nitric oxide; nitrous oxide; samarium; selective catalytic reduction; nitrogen selectivity

1. Introduction

Fossil fuel combustion is the primary source of atmospheric nitrogen oxides (NO_x) and has resulted in severe environmental pollution. One of the most effective methods for controlling NO_x emission is NO_x selective catalytic reduction (SCR) with NH_3 [1–2]. At present, V_2O_5–WO_3(MoO_3)/TiO_2 is widely used as a commercial SCR catalyst. However, the application of the catalyst is limited by the poor activity at low temperature and its narrow operation temperature window of 300–500°C [3–5]. Therefore, novel SCR catalysts achieving high catalytic activity and selectivity at low temperatures must be developed [6–7].

Recently, Mn-based catalysts have attracted the attention of numerous researchers [8–9]. These catalysts exhibit outstanding SCR performance due to the multiple valences and labile oxygen of manganese oxides (Mn_2O_3, Mn_3O_4, and MnO_2) [10]. TiO_2 is a favorable support for Mn-based catalysts [11]. Peña *et al.* [12] studied various transition metal oxides (V, Cr, Mn, Fe, Co, Ni, and Cu) supported on TiO_2 for the SCR of NO with NH_3 and found that the Mn–TiO_2 catalysts achieved the best catalytic performance among these catalysts. However, poor N_2 selectivity limited the application of Mn–TiO_2 catalysts. The decreased N_2 selectivity was due to the overoxidation of NH_3 caused by a strong redox property [13]. To solve these problems, some researchers studied Mn–TiO_2 catalysts modified by various rare metals or transition metals, such as Eu, La, Ce, Fe, Co, and Zr [14–17]. The results indicate that these doped modifying metals can enhance the N_2 selectivity and NO conversion of Mn–TiO_2 catalysts.

The rare metal Sm has been introduced to improve catalytic activity. Casanova *et al.* [18] found that Sm-modified V_2O_5–WO_3–TiO_2–SiO_2 catalysts exhibited excellent SCR performance. Meng *et al.* [19] prepared Sm–Mn mixed oxide catalysts using the co-precipitation method and found that Sm doping clearly influenced the NO conversion of the catalysts. However, the effects of Sm on the N_2 selectivity of Mn–TiO_2 catalysts have not been studied deeply.

In this work, a series of $Sm_xMn_{0.3-x}Ti$ catalysts (x = 0, 0.1, 0.15, 0.2, and 0.3) was prepared to improve N_2 selectivity and catalytic activity. The effects of Sm on the N_2 selectivity of

✉ Corresponding authors: Bolin Zhang E-mail: zhangbolin@ustb.edu.cn;
Shengen Zhang E-mail: zhangshengen@mater.ustb.edu.cn

$Sm_xMn_{0.3-x}Ti$ catalysts were investigated, and the role of Sm in suppressing N_2O generated from different origins was revealed.

2. Experimental

2.1. Catalyst synthesis

A series of $Sm_xMn_{0.3-x}Ti$ catalysts with a Sm/Ti molar ratio of 0, 0.1, 0.15, 0.2, and 0.3 were prepared by co-precipitation. First, appropriate amounts of $Ti(SO_4)_2$, $Sm(NO_3)_3$, and $Mn(NO_3)_2$ (50wt% aqueous solution) were dissolved in deionized water. Second, ammonium hydroxide ($NH_3 \cdot H_2O$, 25wt%) was added slowly to the mixed solution under vigorous stirring until the pH value reached 10. After stirring for 4 h, the obtained precipitate was filtered and washed three times with deionized water. The resulting powder was dried at 90°C for 6 h and finally calcined at 500°C for 2 h.

2.2. Catalyst characterization

The X-ray diffraction (XRD) patterns were recorded on a Rigaku Ultima IV diffractometer (Japan) with Cu K_α radiation (λ = 0.15406 nm). The N_2 adsorption–desorption isotherms were measured on a Quadrasorb SI automated surface area and pore size analyzer (Quantachrome, America). The specific surface area of the sample was calculated by the Brunauer-Emmett-Teller (BET) method. The XPS experiments were performed on a Thermo Escalab 250XI multifunctional photoelectron spectrometer with an Al K_α X-ray source. Sample charging effects were eliminated by collecting the observed spectra with the C 1s binding energy value of 284.6 eV. The O 1s, Mn 2p, Ti 2p, and Sm 3d peaks were deconvoluted by the Gaussian–Lorentzian function with a Shirley background. The temperature-programmed desorption of NH_3 (NH_3-TPD) adsorbed on the catalyst was performed using a programmed temperature chemisorption analyzer (Micromeritics AutoChem1 II 2920, America) equipped with a thermal conductivity detector (TCD). 100 mg catalyst was pretreated with He gas at 300°C and then cooled to room temperature. Subsequently, the catalyst was treated with 10vol% NH_3–He mixed gases (30 mL·min^{-1}) until adsorption equilibrium, and then purged with helium (30 mL·min^{-1}) to remove the adsorbed NH_3. Finally, the samples were heated to 850°C at a linear heating rate of 10°C·min^{-1} under a He atmosphere. The temperature-programmed H_2 reduction (H_2-TPR) experiments were performed using a programmed temperature chemisorption analyzer (Micromeritics AutoChem1 II 2920, America) equipped with a TCD. The catalyst was pretreated with Ar gas at 350°C and then cooled to room temperature. Then, the sample was heated to 800°C at a heating rate of 10°C·min^{-1} with 10vol% H_2–Ar mixed gases (30 mL·min^{-1}). Finally, H_2 consumption in the TPR process was recorded by a TCD. *In situ* diffuse reflectance infrared Fourier transform spectra (DRIFTs) experiments were performed on a Tensor 27 infrared Fourier transform spectrometer (Bruker, Germany) equipped with a Pike DRIFTs cell containing an MCT detector. Before the experiments, the catalyst was pretreated at 300°C for 1 h in a flow of argon and then cooled to 200°C. Then the background spectra were obtained during the cooling process and recorded by subtracting each sample background.

2.3. Catalytic activity measurements

The catalytic activities of these catalysts for NH_3-SCR were measured at 100–300°C under a steady state. In this test, ca. 200 mg of powder catalysts with 40–100 mesh was placed in a fixed quartz reactor (inner diameter of 8 mm) under a flow rate of 300 mL·min^{-1}. The inlet concentrations were composed of 600 ppm NH_3, 600 ppm NO, 5vol% O_2, and N_2 balance. The simulated gas stream was fed into the reactor with a gas hourly space velocity (GHSV) of 36000 h^{-1}. The reactants and products were analyzed by the analyzer online, and the concentrations of NO, N_2O, and O_2 in the outlet flue gas were recorded using an infrared gas analyzer equipped with a professional gas conditioner (Madur Photon II & PGD-100, Austria). The NO conversion and N_2 selectivity were calculated as the following formulas [20–21]:

$$X_{NO} = \left(1 - \frac{c_{NO,out}}{c_{NO,in}}\right) \times 100\% \quad (1)$$

$$S_{N_2} = \left(1 - \frac{2c_{N_2O,out}}{c_{NO,in} - c_{NO,out}}\right) \times 100\% \quad (2)$$

where X_{NO}, S_{N_2}, and c_{NO} are the NO conversion, N_2 selectivity, and NO concentration, respectively. The $c_{NO,in}$, $c_{NO,out}$, and $c_{N_2O,out}$ are the inlet or outlet concentrations of NO_x (NO and N_2O) in this article.

3. Results and discussion

3.1. Catalytic activity and selectivity

Fig. 1(a) shows the relationship between NO conversion and temperature over $Sm_xMn_{0.3-x}Ti$ catalysts. The $Sm_{0.3}Ti$ catalyst exhibited poor catalytic activity with its low NO conversion at 180–300°C. However, the Mn-containing catalysts exhibited superior catalytic activity at the same temperature range. A NO conversion of 100% was obtained at 200°C for Mn-containing catalysts. Peña *et al.* [12] found that with a decrease in Mn, the NO conversion decreased over Mn-based catalysts. However, the results showed that as the Mn load decreased, the NO conversion over $Sm_{0.1}Mn_{0.2}Ti$, $Sm_{0.15}Mn_{0.15}Ti$, and $Sm_{0.2}Mn_{0.1}Ti$ catalysts did not decrease at 180–300°C. The results indicated that adding Sm contributed to catalytic activity.

Fig. 1(b) shows that the N_2 selectivity over the $Mn_{0.3}Ti$ catalyst decreased obviously with increasing temperature. The N_2 selectivity over $Mn_{0.3}Ti$ was less than 60% above 180°C, while it was above 90% at 100–260°C after introducing Sm into the catalysts. Fig. 1(c) shows that the concentration of N_2O over the $Mn_{0.3}Ti$ catalyst increased with temperature and reached 289 ppm at 300°C, which was much higher than that of Sm-modified catalysts. These results implied that adding Sm could enhance the N_2 selectivity.

3.2. Catalytic oxidation of NH_3 and NO

NH_3 and NO catalytic oxidation experiments were per-

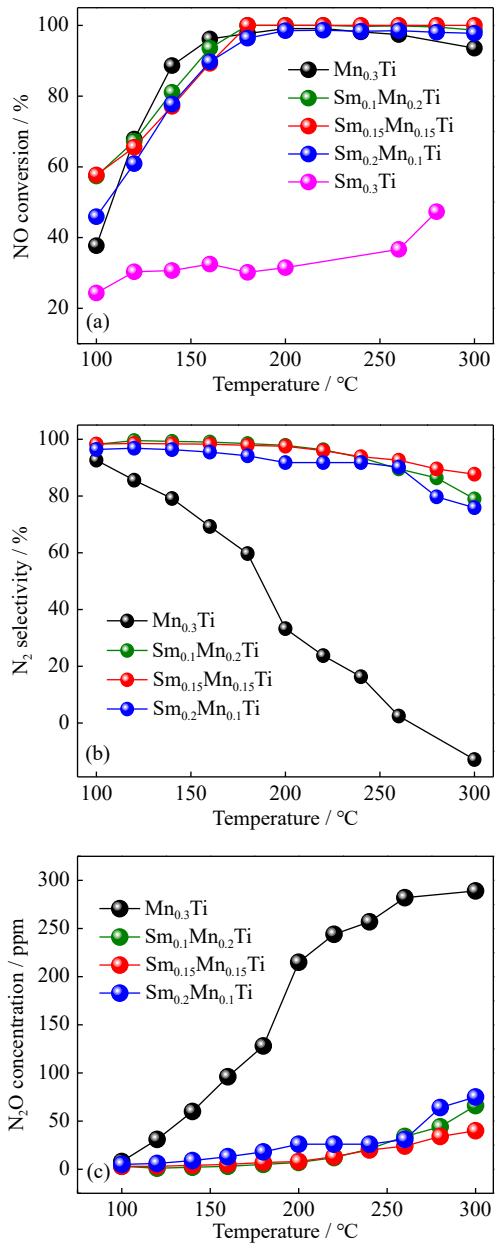

Fig. 1. (a) NO conversion, (b) N_2 selectivity, and (c) N_2O concentration over $Sm_xMn_{0.3-x}Ti$ catalysts (x = 0, 0.1, 0.15, 0.2, and 0.3). Inlet reaction condition: 600 ppm NH_3, 600 ppm NO, 5vol% O_2, and N_2 balance; GHSV = 36000 h^{-1}.

formed to investigate the possible ways for N_2O formation and the processes of NH_3 and NO catalytic oxidation over different catalysts. In the NO oxidation experiment, $Mn_{0.3}Ti$ and $Sm_{0.15}Mn_{0.15}Ti$ catalysts were exposed to NO and O_2. NO could be oxidized to NO_2 by reaction (3) or decomposed to N_2O by reaction (4) [22].

$$2NO + O_2 \rightarrow 2NO_2 \quad (3)$$

$$3NO \rightarrow N_2O + NO_2 \quad (4)$$

Fig. 2(a) shows that little NO decomposed into N_2O by reaction (4) over the catalysts. In contrast, a small amount of NO was oxidized to NO_2 over different catalysts (Fig. 2(b)). Some researchers reported that a small amount of NO_2 involved in a fast-SCR process improved catalytic [22–23]. As shown in Fig. 2(b), The NO_2 concentration of $Mn_{0.3}Ti$ and

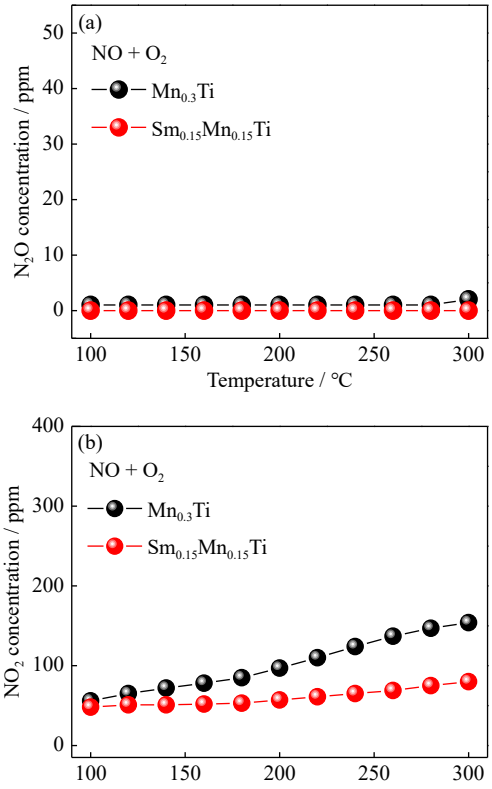

Fig. 2. (a) N_2O and (b) NO_2 formation from NO catalytic oxidation over $Mn_{0.3}Ti$ and $Sm_{0.15}Mn_{0.15}Ti$ catalysts. Inlet reaction condition: 600 ppm NH_3, 600 ppm NO, 5vol% O_2, and N_2 balance; GHSV = 36000 h^{-1}.

$Sm_{0.15}Mn_{0.15}Ti$ catalysts reached 50 ppm at 180–300°C. These catalysts could catalytically oxidate a part of NO to NO_2, which contributed to the fast-SCR process and facilitated superior $deNO_x$ activity.

In the NH_3 oxidation experiment, $Mn_{0.3}Ti$ and $Sm_{0.15}Mn_{0.15}Ti$ catalysts were exposed to NH_3 and O_2. NH_3 could be oxidized to N_2O by reaction (5), NO by reaction (6), and NO_2 by reaction (7) [23–24].

$$4NH_3 + 4O_2 \rightarrow 2N_2O + 6H_2O \quad (5)$$

$$4NH_3 + 5O_2 \rightarrow 4NO + 6H_2O \quad (6)$$

$$4NH_3 + 7O_2 \rightarrow 4NO_2 + 6H_2O \quad (7)$$

At 150–300°C, increased N_2O concentration was observed with increasing temperature (Fig. 3(a)). Then, the N_2O concentration of $Mn_{0.3}Ti$ increased up to 165 ppm at 240°C. From the SCR activity and NH_3 oxidation results, the poor N_2 selectivity over $Mn_{0.3}Ti$ catalyst at 150–300°C was mainly due to NH_3 overoxidation. Furthermore, the N_2O concentration over $Sm_{0.15}Mn_{0.15}Ti$ was below 48 ppm at 240°C, which was less than that over $Mn_{0.3}Ti$. This result indicated that introducing Sm obviously suppressed the pathway to N_2O from the direct oxidation of NH_3.

Fig. 3(b) and (c) shows low concentrations of NO and NO_2 over $Mn_{0.3}Ti$ and $Sm_{0.15}Mn_{0.15}Ti$ catalysts at 160–300°C. This result indicated that little NH_3 was catalytically oxidized to NO and NO_2; thus, the presence of Sm inhibited the NH_3 catalytic oxidation.

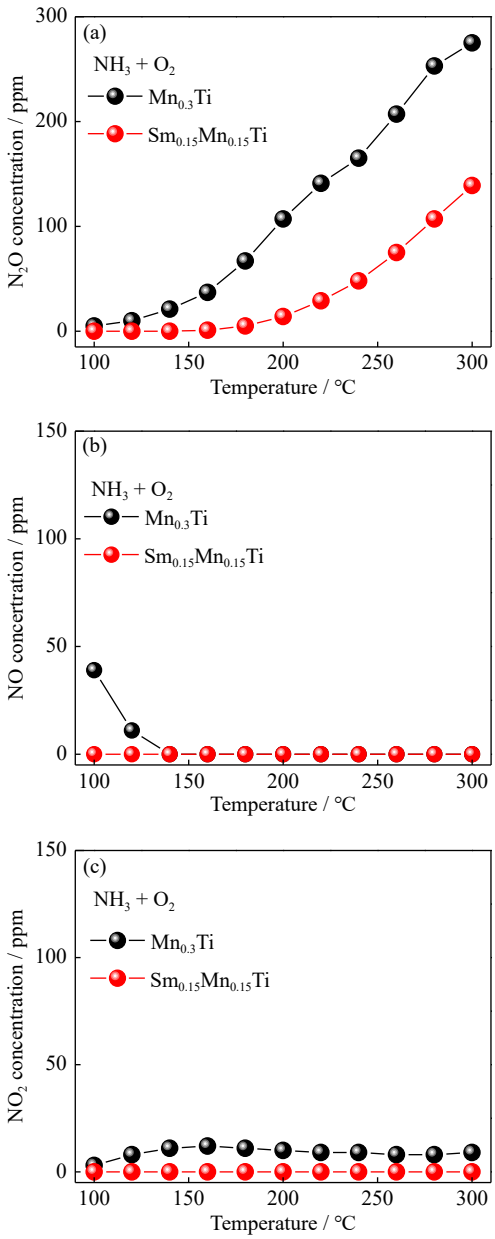

Fig. 3. (a) N_2O, (b) NO, and (c) NO_2 formation from NH_3 catalytic oxidation over $Mn_{0.3}Ti$ and $Sm_{0.15}Mn_{0.15}Ti$ catalysts. Inlet reaction condition: 600 ppm NH_3, 600 ppm NO, 5vol% O_2, and N_2 balance; GHSV = 36000 h^{-1}.

3.3. XRD and N_2 adsorption–desorption analysis

Fig. 4 shows the powder XRD patterns of different catalysts. The presence of the TiO_2 phase (PDF card No. 21–1276) and the Mn_2O_3 phase (PDF card No. 41–1442) was observed on the $Mn_{0.3}Ti$ catalyst [11]. No additional diffraction peaks of Sm, Mn, and Ti species were observed for $Sm_xMn_{0.3-x}Ti$ catalysts (x = 0.1, 0.15, 0.2, and 0.3). These results imply that the crystallization of TiO_2 and Mn_2O_3 phases was suppressed over the Sm-doped MnTi catalyst [25]. Because of the strong interaction between Sm-doped manganese oxides, the catalytic activity was obviously improved.

Table 1 shows the BET specific surface areas and pore structures of different catalysts. For the $Mn_{0.3}Ti$ catalyst, the BET specific surface area was only 152.19 $m^2 \cdot g^{-1}$. After Sm

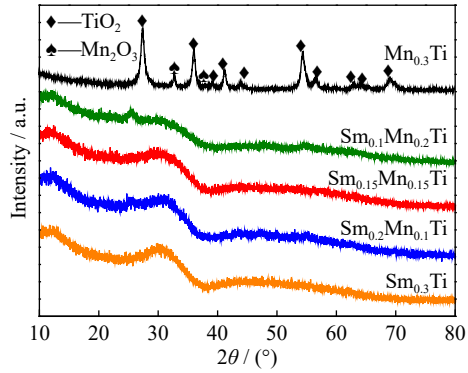

Fig. 4. XRD patterns of different catalysts.

was introduced, the BET specific surface area remarkably increased to over 240 $m^2 \cdot g^{-1}$ for $Sm_xMn_{0.3-x}Ti$ catalysts (x = 0.1, 0.15, and 0.2). The BET specific surface areas of $Sm_{0.1}Mn_{0.2}Ti$, $Sm_{0.15}Mn_{0.15}Ti$, and $Sm_{0.2}Mn_{0.1}Ti$ were 263.92, 241.69, and 267.31 $m^2 \cdot g^{-1}$, respectively. The larger specific surface area improved the effective contact area between active species and reactants on catalysts. As shown in Table 1, the average pore size of the Sm-modified catalysts was less than 14 nm. The decrease in average pore diameter should prolong the residence time of effective contacts between active species with the reactants, thus effectively promoting the NH_3-SCR reaction. Nitrogen adsorption–desorption analysis results indicated the presence of mesoporous in the $Sm_xMn_{0.3-x}Ti$ catalysts (x = 0, 0.1, 0.15, 0.2, and 0.3) (Figs. S1 and S2) [26]. When the most probable pore-size distribution decreased to ~4 nm for the other catalysts doping Sm, it might prolong the reaction time of the NH_3-SCR reaction in pore size.

Table 1. BET specific surface area and pore structure results of different catalysts

Sample	BET surface area / ($m^2 \cdot g^{-1}$)	Average pore diameter / nm	Pore volume / ($cm^3 \cdot g^{-1}$)
$Mn_{0.3}Ti$	152.19	21.45	0.61
$Sm_{0.1}Mn_{0.2}Ti$	263.92	13.77	0.70
$Sm_{0.15}Mn_{0.15}Ti$	241.69	11.30	0.55
$Sm_{0.2}Mn_{0.1}Ti$	267.31	11.48	0.59
$Sm_{0.3}Ti$	227.01	14.86	0.64

3.4. XPS analysis

X-ray photoelectron spectroscopy (XPS) analysis was used to study the surface element compositions and chemical states. The Gaussian–Lorentz function was used to deconvolve the XPS spectra of Mn 2p, Sm 3d, and O 1s. Fig. S3 shows the deconvoluted results of different elements in total XPS spectrum. The XPS spectra of Mn 2p, Sm 3d, and O 1s were obtained from total XPS spectra (Fig. 5). Table 2 shows the results of the relative percentages of O_β/O, Mn^{4+}/Mn, and Sm^{3+}/Sm calculated by the area ratio of the corresponding characteristic peaks, and the results of the surface atomic concentration ratios of Mn, Sm, and O on different catalysts.

Fig. 5(a) shows the deconvoluted Mn 2p XPS results of different catalysts. The XPS spectra binding energies

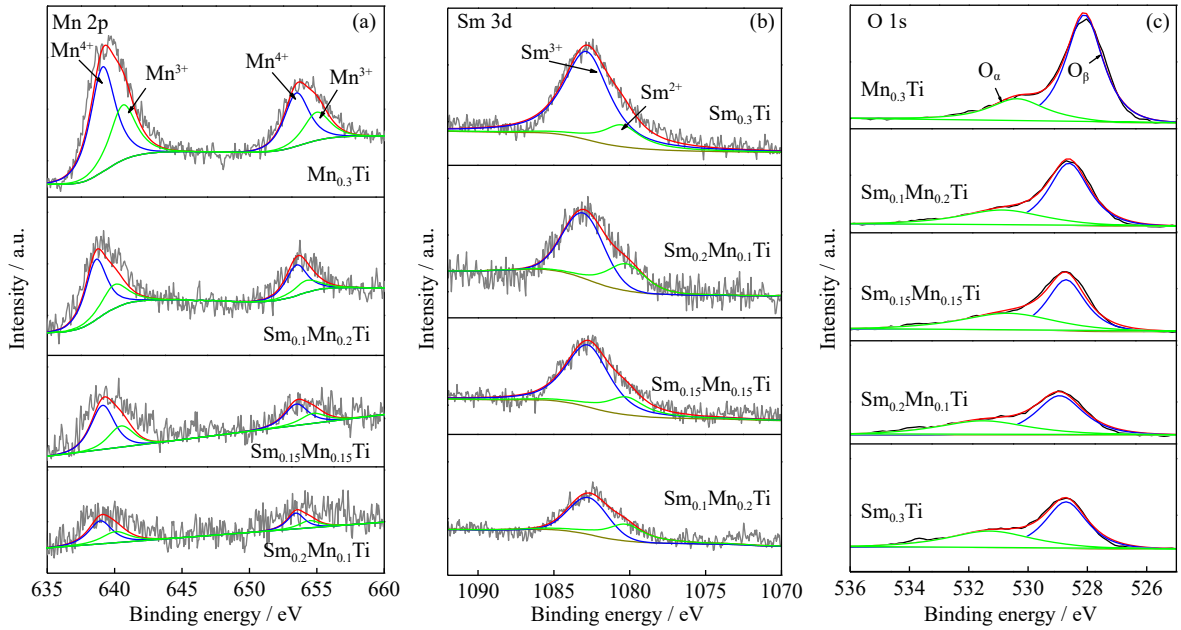

Fig. 5. XPS spectra of different catalysts: (a) Mn 2p; (b) Sm 3d; (c) O 1s.

Table 2. Elemental surface analysis of the different catalysts (by XPS)

Sample	Surface element content / at%				Relative atomic ratio of surface element valence state / at%		
	Ti	O	Mn	Sm	$O_\beta/(O_\beta + O_\alpha)$	Mn^{4+}/Mn	Sm^{3+}/Sm
$Mn_{0.3}Ti$	22.75	68.12	9.13	—	21.27	64.68	—
$Sm_{0.1}Mn_{0.2}Ti$	23.71	68.79	4.54	2.96	31.86	68.02	59.88
$Sm_{0.15}Mn_{0.15}Ti$	24.24	69.06	3.30	3.40	44.11	66.81	76.77
$Sm_{0.2}Mn_{0.1}Ti$	23.35	68.80	3.31	4.53	40.65	64.44	68.14
$Sm_{0.3}Ti$	23.77	70.69	—	5.53	41.49	—	81.26

ascribed to the Mn^{4+} and Mn^{3+} species of Mn 2p [17,27] were (643.5 ± 0.2) eV and (641.5 ± 0.2) eV, respectively. Table 3 shows the atomic ratio of Mn and concentrations of Mn^{4+} and Sm^{3+} for catalysts. For the $Sm_{0.15}Mn_{0.15}Ti$ catalyst, the relative surface atomic ratio of Mn/Ti was 0.14, and the surface element concentrations of Mn^{4+} was 2.20at%. However, for the $Mn_{0.3}Ti$ catalyst, the relative surface atomic ratio of Mn/Ti was increased to 0.40, and the surface element concentrations of Mn^{4+} was increased to 5.91at%. Previous research showed that an increase in Mn^{4+} species would improve the redox property and decrease the N_2 selectivity for the overoxidation of NH_3 [12]. For the present Sm-modified catalysts, the decrease in Mn^{4+} species improved the N_2 selectivity for the decreased redox property. Previous research also showed that the catalytic activity decreased with a decrease in Mn loading over Mn-based catalysts [12]. However, the catalytic activity did not decrease over $Sm_{0.15}Mn_{0.15}Ti$ with the decrease of Mn loading.

Fig. 5(b) shows the Sm 3d XPS spectra of the catalyst surface. The XPS spectra binding energies ascribed to the Sm^{3+} and Sm^{2+} species of Sm 3d [28–29] were 1083.3 and 1080.7 eV, respectively. As shown in Table 2, for the $Sm_{0.15}Mn_{0.15}Ti$ catalyst, the surface atomic ratio of Sm^{3+}/Sm was 76.77at%, which was much higher than that of other catalysts. The higher atomic ratio of Sm^{3+}/Sm should increase oxygen vacancies, thus promoting the SCR reaction.

Fig. 5(c) shows the O 1s XPS spectra of different catalysts. The peaks at 531.27 and 529.62 eV correspond to lat-

Table 3. Atomic ratios of Mn and concentrations of Mn^{4+} and Sm^{3+} for catalysts (by XPS)

Sample	Bulk and surface relative atomic ratio		Surface element content / at%	
	[a]Mn/Ti	[b]Mn/Ti	[c]Mn^{4+}	[c]Sm^{3+}
$Mn_{0.3}Ti$	0.30	0.40	5.91	—
$Sm_{0.1}Mn_{0.2}Ti$	0.20	0.19	3.09	1.77
$Sm_{0.15}Mn_{0.15}Ti$	0.15	0.14	2.20	2.61
$Sm_{0.2}Mn_{0.1}Ti$	0.10	0.14	2.13	3.09
$Sm_{0.3}Ti$	—	—	—	4.49

Note: [a]bulk atomic ratio of prepared catalysts as designed; [b]surface relative atomic ratio of catalyst; [c]surface element concentrations of Mn^{4+} and Sm^{3+} were according to the surface element concentrations and the relative atomic ratio of surface element valence states in Table 2.

tice oxygen O_α and surface-adsorbed oxygen O_β, respectively [25,30]. As shown in Table 2, the relative atomic ratio of O_β/O was 44.11at% for the $Sm_{0.15}Mn_{0.15}Ti$ catalyst, which was much higher than that of other catalysts (21.27at%, 31.86at%, and 40.65at% for $Mn_{0.3}Ti$, $Sm_{0.1}Mn_{0.2}Ti$, and $Sm_{0.2}Mn_{0.1}Ti$ catalysts, respectively). This result indicated that introducing Sm increased the concentration of surface-adsorbed oxygen O_β, which led to an increase in catalytic activity.

These XPS analysis results indicated that the co-doped Sm and Mn catalysts achieved a superior performance of NO conversion and N_2 selectivity. Previous research showed that the electron transfer between Mn and Sm promoted the redox cycle of $Mn^{4+} + Sm^{2+} \leftrightarrow Mn^{3+} + Sm^{3+}$ in the NH_3-SCR process [20,26]. This route has promise for designing Mn and Sm co-doped catalysts that achieve high N_2 selectivity and NO conversion.

3.5. NH_3-TPD analysis

The acidic sites distribution and total acidity on the catalyst surface was determined using NH_3-TPD analysis. The total acidity on catalyst surface was an important factor for NH_3 adsorption, which also affected the catalytic activity of the NH_3-SCR reaction. A higher desorption temperature led to stronger adsorption sites, which absorbed more NH_3 [28]. As shown in Fig. 6(a), the desorption peaks attributed to the strongly acidic sites of the catalysts were at 260, 357, 352, and 329°C [31]. This result indicated that the presence of Sm shifted the desorption peaks to a higher temperature, which may be attributed to stronger acidic adsorption sites adsorbing more NH_3.

The total acidity of the $Sm_{0.15}Mn_{0.15}Ti$ or $Mn_{0.3}Ti$ catalyst is related to the acid desorption peak areas [20]. Comparing the desorption peak areas at 352 and 260°C, Fig. 6(b) shows that the $Sm_{0.15}Mn_{0.15}Ti$ catalyst obtained a larger peak area at the higher temperature of 352°C. This result indicated that the number of strongly acidic sites increased for the Sm-modified catalysts. The presence of Sm increased not only the strength but also the total number of acidic sites on the catalyst surface. These results improved the adsorption and activation of NH_3 for the catalysts, further contributing to catalytic activity.

3.6. H_2-TPR analysis

The redox properties of $Sm_xMn_{0.3-x}Ti$ catalysts (x = 0, 0.1, 0.15, 0.2, and 0.3) were investigated through H_2-TPR analysis. The analysis results are shown in Fig. 7. The peaks at 270–320°C (peak I) and 365–386°C (peak II) were attributed to the reduction reactions of $MnO_2 \rightarrow Mn_2O_3$ and $MnO_2/Mn_2O_3 \rightarrow Mn_3O_4$ [8,29]. The peaks at 550–700°C might be assigned to the reduction of Mn_3O_4 ($Mn_3O_4 \rightarrow MnO$) and Ti^{4+} species [23,31]. The reduction peaks of $Sm_{0.3}Ti$ at 581 and 668°C might be due to TiO_2 reduction. For the $Mn_{0.3}Ti$ catalyst, the strong peaks at 270 and 368°C were assigned to the reduction of MnO_x species, such that MnO_2 was reduced to Mn_2O_3, and then Mn_2O_3 was reduced to Mn_3O_4. The reduction peaks of $Sm_{0.1}Mn_{0.2}Ti$ (peaks I and II) and $Sm_{0.15}Mn_{0.15}Ti$ (peak II) shifted to higher temperatures. After Sm was introduced, the reduction temperatures of these catalysts increased. This result might be due to the suppression of metal oxide reduction by the Sm–O–Mn bond formation of the catalysts. For the $Sm_{0.15}Mn_{0.15}Ti$ and $Sm_{0.2}Mn_{0.1}Ti$ catalysts, peak I disappeared and the peak II intensity decreased. This result was due to the decrease in Mn^{4+} and the redox properties of the catalysts, which have been confirmed by the XPS results. The H_2-TPR results shows the H_2 consumptions of different catalysts, which were calculated according to the reduction peaks. The H_2 consumption of the $Sm_{0.1}Mn_{0.2}Ti$, $Sm_{0.15}Mn_{0.15}Ti$, and $Sm_{0.2}Mn_{0.1}Ti$ catalysts was 0.45, 0.30, and 0.45 mmol·g^{-1}, respectively, which was much lower than that of $Mn_{0.3}Ti$ (1.16 mmol·g^{-1}). The high H_2 consumption of $Mn_{0.3}Ti$ might be related to the high Mn^{4+} content. However, due to the decrease of Mn^{4+} content in $Sm_{0.15}Mn_{0.15}Ti$, the H_2 consumption and redox property of the catalyst decreased. The decreased redox property of $Sm_{0.15}Mn_{0.15}Ti$ suppressed N_2O formation from NH_3 oxidation.

3.7. *In situ* DRIFTs analysis

To study its adsorption behavior and reaction mechanism, Fig. 8 recorded *in situ* DRIFTs of the adsorption of NH_3 and NO + O_2 on $Sm_{0.15}Mn_{0.15}Ti$ catalyst at 200°C. In the spectra of

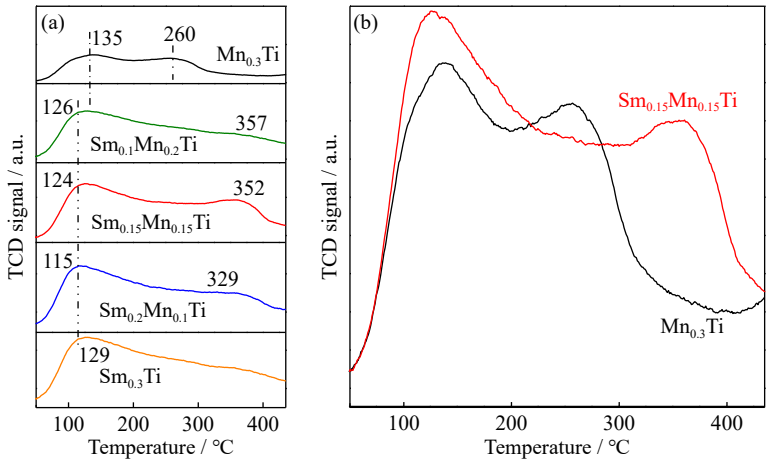

Fig. 6. NH_3-TPD profiles of (a) $Sm_xMn_{0.3-x}Ti$ catalysts (x = 0, 0.1, 0.15, 0.2, and 0.3) and (b) $Sm_{0.15}Mn_{0.15}Ti$ and $Mn_{0.3}Ti$ catalysts.

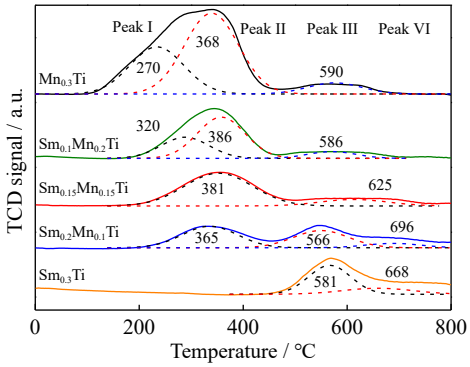

Fig. 7. H_2-TPR profiles of different catalysts.

NO + O_2 co-adsorption on the $Sm_{0.15}Mn_{0.15}Ti$ catalyst (Fig. 8(a)), several vibrational bands were observed at 1000–1800 cm^{-1}: adsorbed NO_2 (1612 cm^{-1}), bidentate nitrate (1574 and 1564 cm^{-1}), linear nitrite (1438 cm^{-1}), M–NO_2 nitro species (1348 cm^{-1}), and bridging bidentate nitrates (1240 and 1194 cm^{-1}) [32–33]. After 10 min, new bands at 1612 and 1240 cm^{-1} became apparent and were enhanced with increasing adsorption time. The band at 1574 cm^{-1} (shifted to 1564 cm^{-1} with an increase in flow time) increased in intensity with flow time until 40 min. Because linear nitrite could be transformed into NO_2 species [33], the peak at 1438 cm^{-1} ascribed to linear nitrite decreased with the adsorption time.

Fig. 8(b) shows the spectra of NH_3 reacted with pre-adsorbed NO + O_2 at 200°C. The $Sm_{0.15}Mn_{0.15}Ti$ catalyst was mainly covered by nitrate species, such as adsorbed NO_2 (1612 cm^{-1}), bidentate nitrate (1564 cm^{-1}), linear nitrite (1438 cm^{-1}), M–NO_2 nitro species (1348 cm^{-1}), and bridging bidentate nitrates (1240 cm^{-1}). When the catalyst was exposed to NH_3 for 10 min, all the coordinated NH_3 (3364, 3256, 1261, and 1195 cm^{-1}) at Lewis acid sites appeared immediately [32]. After NH_3 was introduced, the bridging bidentate nitrates (1240 cm^{-1}) gradually diminished, and the coordinated NH_3 (1261 cm^{-1}) was formed, which indicated that the SCR reaction could occur between the bridging bidentate nitrates and coordinated NH_3 [32,34]. The adsorbed NO_2 (1612 cm^{-1}) substantially decreased, which indicated the reaction between the activated NH_3 and NO species. Some researchers found that adsorbed NO_2 could react with NH_4^+ to form $NO_2[NH_4^+]_2$ and then react with NO to form N_2 and H_2O [35]. The activated NH_4^+ at Brønsted acid sites was not observed, possibly having been consumed by the reaction with NO_2. In addition, the band at 1564 cm^{-1} for bidentate nitrate shifted to 1528 cm^{-1}. This result indicated that NH_3 could snatch an adsorption site from bidentate nitrate to form activated NH_4^+ at Brønsted acid sites, and then the bidentate nitrate transformed to monodentate nitrate [33,35].

Fig. 8(c) shows *in situ* DRIFTs of the adsorption of NH_3 on the $Sm_{0.15}Mn_{0.15}Ti$ catalyst at 200°C. The bands detected at 3358 and 3254 cm^{-1} were attributed to the N–H stretching vibrations of coordinated NH_3 [36–37]. The bands at 1261 and 1194 cm^{-1} were attributed to coordinated NH_3 at Lewis acid sites [36]. The bidentate nitrate at 1528 cm^{-1} might be formed by the oxidation of NH_3 on the catalyst surface. When NO + O_2 was introduced to the pre-adsorbed NH_3 catalyst (Fig. 8(d)), all the coordinated NH_3 were detected within 1 min but decreased within 10 min. After NO + O_2 was introduced for 10 min, all the bands for coordinated NH_3 disap-

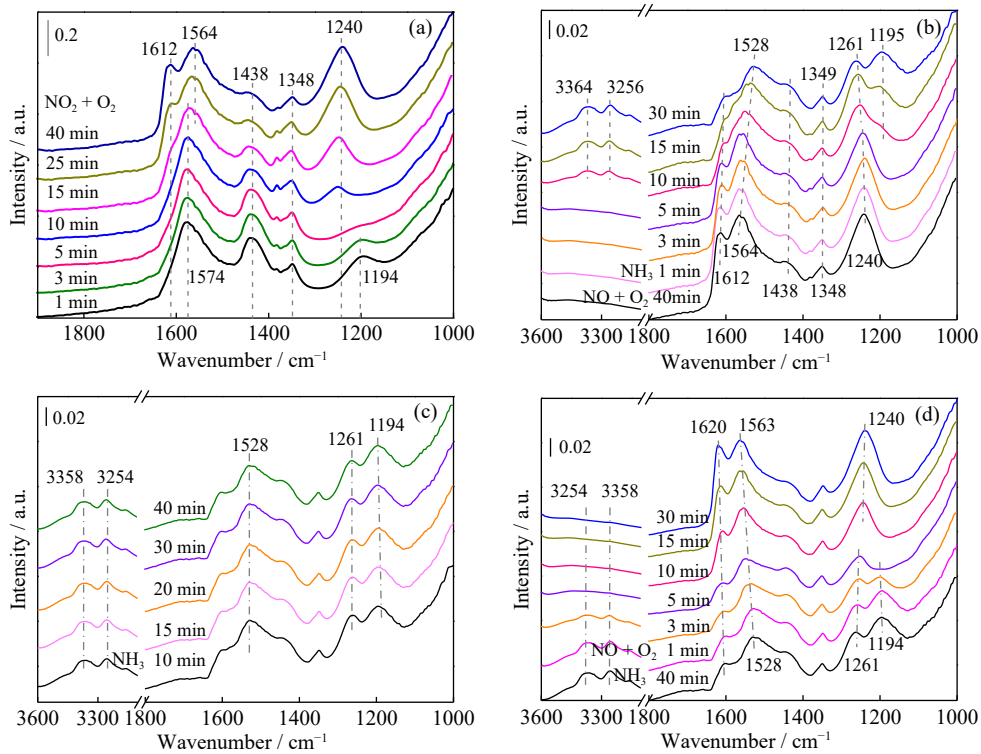

Fig. 8. *In situ* DRIFTs of (a) NO + O_2 adsorption, (b) NH_3 reacted with pre-adsorbed NO + O_2, (c) NH_3 adsorption, and (d) NO + O_2 reacted with pre-adsorbed NH_3 over the $Sm_{0.15}Mn_{0.15}Ti$ catalyst at 200°C.

peared, and a new band at 1240 cm^{-1} attributed to bridging nitrate appeared and increased with time. The band at 1528 cm^{-1} shifted to 1563 cm^{-1} because monodentate nitrate transformed into the more stable bidentate nitrate [36]. These results indicated that coordinated NH_3 species could directly react with gaseous NO on the catalyst, indicating that the $Sm_{0.15}Mn_{0.15}Ti$ catalyst followed the Eley–Rideal (E–R) mechanism.

4. Discussion

4.1. Explanation for high N_2 selectivity

Inhibition N_2O formation is a feasible way to improve catalytic N_2 selectivity [24,37]. Salazar *et al.* [38] demonstrated that one of the two nitrogen atoms in N_2O was obtained from NH_3 and the other originated from NO. The possible pathways of N_2O formation were as follows: i) NO decomposition by reaction (4), ii) NH_3 oxidation by reaction (5), iii) nonselective catalytic reduction (NSCR) of NH_3 with NO or NO_2 by reaction (8), and reaction (9) [15–16].

$$4NH_3 + 4NO + 3O_2 \rightarrow 4N_2O + 6H_2O \quad (8)$$

$$4NH_3 + 4NO_2 + O_2 \rightarrow 4N_2O + 6H_2O \quad (9)$$

Fig. 9 shows the origin of N_2O over the $Sm_{0.15}Mn_{0.15}Ti$ and $Mn_{0.3}Ti$ catalysts from the possible pathways. The NO catalytic oxidation results indicated that little N_2O originated from NO decomposition. This finding indicated that the NO decomposition reaction was not the way to produce N_2O over the catalysts. The N_2O produced by the NH_3 oxidation accounted for the majority of the total N_2O production (Fig. 9(a)). This finding indicated that the N_2O on the $Mn_{0.3}Ti$ catalyst was mainly generated from direct NH_3 oxidation. The other pathways to generate N_2O were the reaction of NO and NH_3 by reaction (8) or reaction (9). Among the different N_2O source pathways, N_2O production was lower over $Sm_{0.15}Mn_{0.15}Ti$ than over $Mn_{0.3}Ti$. After Sm was introduced, the N_2O from NH_3 oxidation and nonselective catalytic reduction (reactions (8) and (9)) was obviously suppressed, which corresponds to high N_2 selectivity.

The *in situ* DRIFTs study showed that bridging bidentate nitrates could react with coordinated NH_3. The NH_3 was oxidized to form NH_2 species. Then, the NH_2 species reacted with the bridging bidentate nitrate to generate N_2 and H_2O. However, if the NH_2 was further oxidized to NH species, the NH could reduce bridging bidentate nitrate to generate the undesired by-product N_2O. The process of NH_2 oxidation to NH was suppressed over the $Sm_{0.15}Mn_{0.15}Ti$ catalyst. Combined with the XPS and H_2-TPR analysis results, the presence of Sm induced a higher reduction temperature and lower H_2 consumption (0.3 $mmol \cdot g^{-1}$) for the $Sm_{0.15}Mn_{0.15}Ti$ catalyst. It might be concluded that Sm–O–Mn bond formation and the decrease in Mn^{4+} species weakened the redox property of the catalyst. The decreased redox property suppressed N_2O formation from the reaction between NH and the bridging bidentate nitrate in NSCR. The process of NH_3 oxidation to N_2O was also suppressed. N_2O formation was limited over Sm-doped catalysts, thus, high N_2 selectivity was

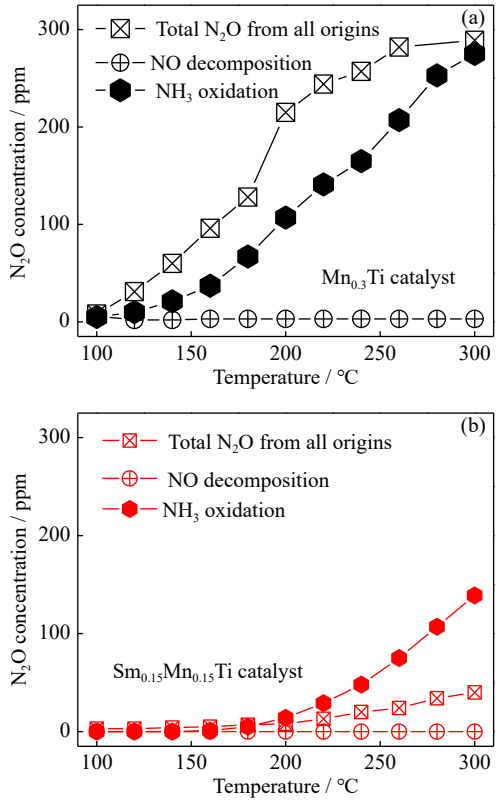

Fig. 9. N_2O concentration from the different origins over (a) $Mn_{0.3}Ti$ and (b) $Sm_{0.15}Mn_{0.15}Ti$ catalysts. Inlet reaction condition: 600 ppm NH_3, 600 ppm NO (total N_2O from all origins), 600 ppm NH_3 (NH_3 catalytic oxidation process), 600 ppm NO (NO catalytic oxidation process), 5vol% O_2, and N_2 balance; GHSV = 36000 h^{-1}.

obtained. Introducing Sm also brought a series of effects, such as increasing the BET specific surface area from 152.2 to 241.7 $m^2 \cdot g^{-1}$ and increasing the strength and population of the surface acidic sites, which clearly contributed to 100% NO conversion and above 87% N_2 selectivity at 180–300°C.

4.2. SCR reaction mechanism

A plausible mechanism for the NH_3-SCR reaction of the $Sm_{0.15}Mn_{0.15}Ti$ catalyst was also discussed. In general, the typical NH_3-SCR process occurred through standard-SCR (reaction (10)) and fast-SCR (reaction (11)) [26,38].

$$4NH_3 + 4NO + O_2 \rightarrow 4N_2 + 6H_2O \quad (10)$$

$$4NH_3 + 2NO + 2NO_2 \rightarrow 4N_2 + 6H_2O \quad (11)$$

The generation of NO_2 in the process of fast-SCR played a crucial role. The process of fast-SCR was improved by the formation of a small amount of NO_2. This finding indicated that the process of selective catalytic reduction of NO_x with NH_3 mainly occurred with fast-SCR but not standard-SCR. *In situ* DRIFTs analysis showed that the fast-SCR reaction might occur between adsorbed NO_2 and NH_4^+ as the following specific reaction steps (reactions (12) to (15)):

$$NH_3(g) \rightarrow NH_3(a) \quad (12)$$

$$NH_3(a) + H^+ \rightarrow NH_4^+ \quad (13)$$

$$NO_2(a) + 2NH_4^+ \rightarrow NO_2[NH_4^+]_2 \quad (14)$$

$$NO_2[NH_4^+]_2 + NO \rightarrow 2N_2 + 3H_2O + 2H^+ \quad (15)$$

where g and a mean gaseous and adsorbed, respectively.

In addition, another reaction mechanism (the E–R mechanism) was also available to the $Sm_{0.15}Mn_{0.15}Ti$ catalyst. The coordinated NH_3 at the Lewis acid site could be activated to form NH_2 species (reaction (16)) and then reacted with gaseous NO to form NH_2NO (reaction (17)). Finally, the intermediate product NH_2NO decomposed to generate N_2 and H_2O (reaction (18)).

$$NH_3(g) \rightarrow NH_3(a) \rightarrow NH_2(a) + H^+ + e^- \quad (16)$$

$$NH_2(a) + NO \rightarrow NH_2NO \quad (17)$$

$$NH_2NO \rightarrow N_2 + H_2O \quad (18)$$

The mechanism of the NH_3-SCR reaction of the $Sm_{0.15}Mn_{0.15}Ti$ catalyst was also studied. On the basis of the kinetic analysis method of Yang *et al.* [39], the contributions of the Langmuir–Hinshelwood (L–H) and E–R mechanisms were determined by changing the concentrations of NO and NH_3 at the inlet. According to this method, if the SCR reaction over the catalysts followed the E–R mechanism, the NO conversion would not decrease with the NO and NH_3 concentrations increasing from 600 to 1200 ppm; if it followed the L–H mechanism, the NO conversion would be halved when the NO concentration doubled.

Fig. 10 shows the results of NO conversion on the $Mn_{0.3}Ti$ and $Sm_{0.15}Mn_{0.15}Ti$ catalysts with the changing inlet flue concentrations of NO and NH_3. To ensure sufficient SCR reaction, the inlet flue concentration of NH_3 was equal to that of NO. As shown in Fig. 10(a), the NO conversion over $Mn_{0.3}Ti$ did not halve below 240°C. This result indicated that the NH_3-SCR reaction of the catalyst followed the L–H mechanism and the E–R mechanism below 240°C. Furthermore, the contribution of the E–R mechanism increased with temperature and was dominant above 240°C. With the inlet flue concentrations of NO and NH_3 changed, the NO conversion over the $Sm_{0.15}Mn_{0.15}Ti$ catalyst did not decrease (Fig. 10(b)). This result indicated that the E–R mechanism was dominant in the NH_3-SCR reaction of the $Sm_{0.15}Mn_{0.15}Ti$ catalyst.

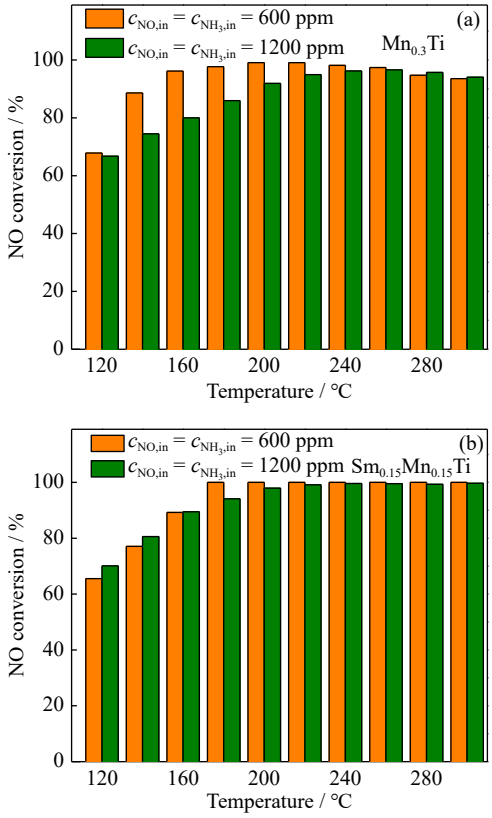

Fig. 10. Influence of NO inlet concentration on the SCR activity over (a) $Mn_{0.3}Ti$ and (b) $Sm_{0.15}Mn_{0.15}Ti$ catalysts at 100–300°C ($c_{NH_3,in}$—Inlet concentration of NH_3). Inlet reaction condition: 600 ppm NH_3, 600 ppm NO, 1200 ppm NH_3, 1200 ppm NO, 5vol% O_2, and N_2 balance; GHSV = 36000 h^{-1}.

In situ DRIFTs results showed that the NH_3-SCR reaction over the $Sm_{0.15}Mn_{0.15}Ti$ catalyst was co-controlled by the E–R and L–H mechanisms. Combined with the above results, the NH_3-SCR reaction of $Sm_{0.15}Mn_{0.15}Ti$ catalysis was mainly dominated by the E–R mechanism.

5. Conclusion

In this work, a series of $Sm_xMn_{0.3-x}Ti$ catalysts (x = 0, 0.1, 0.15, 0.2, and 0.3) was prepared. The effects of Sm on the N_2 selectivity and catalytic activity were investigated. At 180–300°C, the catalysts achieve 100% NO conversion and above 87% N_2 selectivity with little N_2O produced. The N_2O mainly originates from the direct oxidation of NH_3 and the nonselective catalytic reduction of NH_3 with NO. For the $Sm_{0.15}Mn_{0.15}Ti$ catalyst, introducing Sm induces the decreased Mn^{4+} species, a higher reduction temperature and lower H_2 consumption (0.3 mmol·g^{-1}). This weakens the redox property, thus improving the N_2 selectivity. Introducing Sm brings a series of effects, such as reducing the crystallization of TiO_2 and Mn_2O_3 phases, increasing the BET specific surface area from 152.2 to 241.7 $m^2 \cdot g^{-1}$, increasing the surface-adsorbed oxygen, and increasing the strength and population of the surface acidic sites, which clearly improve NH_3-SCR activity. The synergistic effect of the redox cycle of $Sm^{3+} + Mn^{3+} \leftrightarrow Sm^{2+} + Mn^{4+}$ is also found to improve SCR activity. *In situ* DRIFTs results show that the NH_3-SCR reaction over $Sm_{0.15}Mn_{0.15}Ti$ catalysis is mainly controlled by the E–R mechanism at 100–300°C.

Acknowledgements

This work was sponsored by the National Key R&D Program of China (Nos. 2021YFC1910504, 2019YFC1907101, and 2019YFC1907103), the Key R&D Program of Ningxia Hui Autonomous Region, China (Nos. 2020BCE01001 and 2021BEG01003), the National Natural Science Foundation of China (Nos. U2002212, 51672024, 52102058, and 52204414), the Xijiang Innovation and Entrepreneurship Team (No. 2017A0109004), the Fundamental Research Funds for the Central Universities (Nos. FRF-TP-20-097A1Z and FRF-TP-20-031A1), and the Foshan Science and Technology Innovation Special Foundation (No. BK22BE001).

Conflict of Interest

The authors declare no conflict of interest.

Supplementary Information

The online version contains supplementary material available at https://doi.org/10.1007/s12613-021-2348-5.

References

[1] L. Tang, X.D. Xue, J.B. Qu, Z.F. Mi, X. Bo, X.Y. Chang, S.Y. Wang, S.B. Li, W.G. Cui, and G.X. Dong, Air pollution emissions from Chinese power plants based on the continuous emission monitoring systems network, *Sci. Data*, 7(2020), art. No. 325.

[2] X.M. Wang, X.S. Du, G.P. Yang, J.Y. Xue, Y.R. Chen, and L. Zhang, Chemisorption of NO_2 on V-based SCR catalysts: a fundamental study toward the mechanism of "fast-SCR" reaction, *J. Phys. Chem. C*, 123(2019), No. 33, p. 20451.

[3] X.M. Wang, X.S. Du, L. Zhang, Y.R. Chen, G.P. Yang, and J.Y. Ran, Promotion of NH_4HSO_4 decomposition in NO/NO_2 contained atmosphere at low temperature over V_2O_5–WO_3/TiO_2 catalyst for NO reduction, *Appl. Catal. A*, 559(2018), p. 112.

[4] Y.S. Li, X.S. Leng, S.B. Ma, T.R. Zhang, F.L. Yuan, X.Y. Niu, and Y.J. Zhu, Effects of Mo addition on the NH_3-SCR of NO reaction over $Mo_aMnTi_{10}O_x$ (a = 0.2, 0.4, 0.6 and 0.8): Synergistic action between redox and acidity, *Catal. Today*, 339(2020), p. 254.

[5] M.J. Han, Y.L. Jiao, C.H. Zhou, Y.L. Guo, Y. Guo, G.Z. Lu, L. Wang, and W.C. Zhan, Catalytic activity of Cu–SSZ–13 prepared with different methods for NH_3-SCR reaction, *Rare Met.*, 38(2019), No. 3, p. 210.

[6] B.L. Zhang, S.G. Zhang, and B. Liu, Comparative study on transition element doped Mn–Zr–Ti oxides catalysts for the low-temperature selective catalytic reduction of NO with NH_3, *React. Kinet. Mech. Catal.*, 127(2019), No. 2, p. 637.

[7] W.J. Li, T.Y. Li, and M.Y. Wey, Preferred enhancement of fast-SCR by $Mn/CeSiO_x$ catalyst: study on Ce/Si promotion and shape dependence, *Chem. Eng. J.*, 403(2021), art. No. 126317.

[8] L. Chen, S. Ren, L. Liu, B.X. Su, J. Yang, Z.C. Chen, M.M. Wang, and Q.C. Liu, Catalytic performance over Mn–Ce catalysts for NH3-SCR of NO at low temperature: Different zeolite supports, *J. Environ. Chem. Eng.*, 10(2022), No. 2, p. 107167.

[9] F.M. Wang, B.X. Shen, S.W. Zhu, and Z. Wang, Promotion of Fe and Co doped $Mn–Ce/TiO_2$ catalysts for low temperature NH_3-SCR with SO_2 tolerance, *Fuel*, 249(2019), p. 54.

[10] G. Yang, H.T. Zhao, X. Luo, K.Q. Shi, H.B. Zhao, W.K. Wang, Q.H. Chen, H. Fan, and T. Wu, Promotion effect and mechanism of the addition of Mo on the enhanced low temperature SCR of NO_x by NH_3 over MnO_x/γ–Al_2O_3 catalysts, *Appl. Catal. B*, 245(2019), p. 743.

[11] Y.P. Zhang, T.J. Huang, R. Xiao, H.T. Xu, K. Shen, and C.C. Zhou, A comparative study on the Mn/TiO_2–M(M = Sn, Zr or Al)O_x catalysts for NH_3-SCR reaction at low temperature, *Environ. Technol.*, 39(2018), No. 10, p. 1284.

[12] D.A. Peña, B.S. Uphade, and P.G. Smirniotis, TiO_2-supported metal oxide catalysts for low-temperature selective catalytic reduction of NO with NH_3: I. Evaluation and characterization of first row transition metals, *J. Catal.*, 221(2004), No. 2, p. 421.

[13] B.L. Zhang, M. Liebau, W. Suprun, B. Liu, S.G. Zhang, and R. Gläser, Suppression of N_2O formation by H_2O and SO_2 in the selective catalytic reduction of NO with NH_3 over a Mn/Ti–Si catalyst, *Catal. Sci. Technol.*, 9(2019), No. 17, p. 4759.

[14] B.L. Zhang, L.F. Deng, B. Liu, C.Y. Luo, M. Liebau, S.G. Zhang, and R. Gläser, Synergistic effect of cobalt and niobium in Co_3–Nb–O_x on performance of selective catalytic reduction of NO with NH_3, *Rare Met.*, 41(2022), No. 1, p. 166.

[15] S.J. Yang, F.H. Qi, S.C. Xiong, H. Dang, Y. Liao, P.K. Wong, and J.H. Li, MnO_x supported on Fe–Ti spinel: a novel Mn based low temperature SCR catalyst with a high N_2 selectivity, *Appl. Catal. B*, 181(2016), p. 570.

[16] L. Qiu, J.J. Meng, D.D. Pang, C.L. Zhang, and F. Ouyang, Reaction and characterization of Co and Ce doped Mn/TiO_2 catalysts for low-temperature SCR of NO with NH_3, *Catal. Lett.*, 145(2015), No. 7, p. 1500.

[17] X.J. Yao, L. Chen, J. Cao, Y. Chen, M. Tian, F.M. Yang, J.F. Sun, C.J. Tang, and L. Dong, Enhancing the deNO_x performance of MnO_x/CeO_2–ZrO_2 nanorod catalyst for low-temperature NH_3-SCR by TiO_2 modification, *Chem. Eng. J.*, 369(2019), p. 46.

[18] M. Casanova, K. Schermanz, J. Llorca, and A. Trovarelli, Improved high temperature stability of NH_3-SCR catalysts based on rare earth vanadates supported on TiO_2–WO_3–SiO_2, *Catal. Today*, 184(2012), No. 1, p. 227.

[19] D.M. Meng, W.C. Zhan, Y. Guo, Y.L. Guo, L. Wang, and G.Z. Lu, A highly effective catalyst of Sm–MnO_x for the NH_3-SCR of NO_x at low temperature: promotional role of Sm and its catalytic performance, *ACS Catal.*, 5(2015), No. 10, p. 5973.

[20] Q.L. Chen, R.T. Guo, Q.S. Wang, W.G. Pan, W.H. Wang, N.Z. Yang, C.Z. Lu, and S.X. Wang, The catalytic performance of $Mn/TiWO_x$ catalyst for selective catalytic reduction of NO_x with NH_3, *Fuel*, 181(2016), p. 852.

[21] X.Z. Shao, H.Y. Wang, M.L. Yuan, J. Yang, W.C. Zhan, L. Wang, Y. Guo, and G.Z. Lu, Thermal stability of Si-doped V_2O_5/WO_3–TiO_2 for selective catalytic reduction of NO_x by NH_3, *Rare Met.*, 38(2019), No. 4, p. 292.

[22] D.H. Wang, Q. Yao, C.H. Mou, S.E. Hui, and Y.Q. Niu, New insight into N_2O formation from NH_3 oxidation over MnO_x/TiO_2 catalyst, *Fuel*, 254(2019), art. No. 115719.

[23] S. Yang, S. Xiong, Y. Liao, X. Xiao, F. Qi, Y. Peng, Y. Fu, W. Shan, and J. Li, Mechanism of N_2O formation during the low-temperature selective catalytic reduction of NO with NH_3 over Mn–Fe spinel, *Environ. Sci. Technol.*, 48(2014), No. 17, p. 10354.

[24] H.Y. Chen, Z.H. Wei, M. Kollar, F. Gao, Y.L. Wang, J. Szanyi, and C.H.F. Peden, A comparative study of N_2O formation during the selective catalytic reduction of NO_x with NH_3 on zeolite supported Cu catalysts, *J. Catal.*, 329(2015), p. 490.

[25] P. Lalinda, U.S. Kulathunga, I.J. Lakruwani, D.J. Champa, and M.J. Pradeep, A simple and novel synthetic route to prepare anatase TiO_2 nanopowders from natural ilmenite via the H_3PO_4/NH_3 process, *Int. J. Miner. Metall. Mater.*, 27(2020), No. 6, p. 846.

[26] Z. Amirsardari, A. Dourani, M.A. Amirifar, and N.G. Massoom, Comparative characterization of iridium loading on catalyst assessment under different conditions, *Int. J. Miner. Metall. Mater.*, 28(2021), No. 7, p. 1233.

[27] H. Du, Z.T. Han, Q.M. Wang, Y. Gao, C. Gao, J.M. Dong, and X.X. Pan, Effects of ferric and manganese precursors on catalytic activity of Fe–Mn/TiO_2 catalysts for selective reduction of NO with ammonia at low temperature, *Environ. Sci. Pollut. Res.*, 27(2020), No. 32, p. 40870.

[28] P. Sun, R.T. Guo, S.M. Liu, S.X. Wang, W.G. Pan, M.Y. Li, S.W. Liu, J. Liu, and X. Sun, Enhancement of the low-temperature activity of Ce/TiO_2 catalyst by Sm modification for selective catalytic reduction of NO_x with NH_3, *Mol. Catal.*, 433(2017), p. 224.

[29] D.M. Meng, W.C. Zhan, Y. Guo, Y.L. Guo, Y.S. Wang, L. Wang, and G.Z. Lu, A highly effective catalyst of Sm–Mn mixed oxide for the selective catalytic reduction of NO_x with ammonia: Effect of the calcination temperature, *J. Mol. Catal.*

A: Chem., 420(2016), p. 272.

[30] Q.C. Yu, Y. Deng, F. Wang, Y.B. Feng, X.M. Chen, B. Yang, and D.C. Liu, Preparation of activated ceria and its desulfurization performance, *Int. J. Miner. Metall. Mater.*, 22(2015), No. 9, p. 992.

[31] S.B. Ma, X.Y. Zhao, Y.S. Li, T.R. Zhang, F.L. Yuan, X.Y. Niu, and Y.J. Zhu, Effect of W on the acidity and redox performance of the $Cu_{0.02}Fe_{0.2}W_aTiO_x$ (a = 0.01, 0.02, 0.03) catalysts for NH_3-SCR of NO, *Appl. Catal. B*, 248(2019), p. 226.

[32] B.L. Zhang, M. Liebau, B. Liu, L. Li, S.G. Zhang, and R. Gläser, Selective catalytic reduction of NO_x with NH_3 over Mn–Zr–Ti mixed oxide catalysts, *J. Mater. Sci.*, 54(2019), No. 9, p. 6943.

[33] H. Liu, Z.X. Fan, C.Z. Sun, S.H. Yu, S. Feng, W. Chen, D.Z. Chen, C.J. Tang, F. Gao, and L. Dong, Improved activity and significant SO_2 tolerance of samarium modified CeO_2–TiO_2 catalyst for NO selective catalytic reduction with NH_3, *Appl. Catal. B*, 244(2019), p. 671.

[34] J. Fan, P. Ning, Z.X. Song, X. Liu, L.Y. Wang, J. Wang, H.M. Wang, K.X. Long, and Q.L. Zhang, Mechanistic aspects of NH_3-SCR reaction over CeO_2/TiO_2–ZrO_2–SO_4^{2-} catalyst: *in situ* DRIFTs investigation, *Chem. Eng. J.*, 334(2018), p. 855.

[35] L.L. Li, L. Zhang, K.L. Ma, W.X. Zou, Y. Cao, Y. Xiong, C.J. Tang, and L. Dong, Ultra-low loading of copper modified TiO_2/CeO_2 catalysts for low-temperature selective catalytic reduction of NO by NH_3, *Appl. Catal. B*, 207(2017), p. 366.

[36] S. Ali, L.Q. Chen, Z.B. Li, T.R. Zhang, R. Li, S. Bakhtiar, X.S. Leng, F.L. Yuan, X.Y. Niu, and Y.J. Zhu, Cu_x–$Nb_{1.1-x}$ (x = 0.45, 0.35, 0.25, 0.15) bimetal oxides catalysts for the low temperature selective catalytic reduction of NO with NH_3, *Appl. Catal. B*, 236(2018), p. 25.

[37] Y.J. Kim, H.J. Kwon, I.S. Nam, J.W. Choung, J.K. Kil, H.J. Kim, M.S. Cha, and G.K. Yeo, High deNO_x performance of Mn/TiO_2 catalyst by NH_3, *Catal. Today*, 151(2010), No. 3, p. 244.

[38] M. Salazar, S. Hoffmann, L. Tillmann, V. Singer, R. Becker, and W. Grünert, Hybrid catalysts for the selective catalytic reduction (SCR) of NO by NH_3: Precipitates and physical mixtures, *Appl. Catal. B*, 218(2017), p. 793.

[39] S.J. Yang, C.Z. Wang, J.H. Li, N.Q. Yan, L. Ma, and H.Z. Chang, Low temperature selective catalytic reduction of NO with NH_3 over Mn–Fe spinel: performance, mechanism and kinetic study, *Appl. Catal. B*, 110(2011), p. 71.